Design of an extremely stable low-temperature ultrahigh vacuum scanning tunneling microscope

B. Koslowski,[a] Ch. Dietrich, A. Tschetschetkin, and P. Ziemann
Abteilung Festkörperphysik, Universität Ulm, D-89069 Ulm, Germany

(Received 31 January 2006; accepted 17 May 2006; published online 22 June 2006)

The design and performance of a scanning tunneling microscope operated under ultrahigh vacuum conditions and at low temperature are presented. It allows operating temperatures between 6 K to at least 30 K as well as safe and fast tip/sample transfers. Novel design features resulted in an extremely stable instrument with a noise level of only 0.2 pm_{rms} in the frequency range of 0.5–500 Hz despite a relatively noisy laboratory environment. To demonstrate this behavior, results of test measurements performed on Au(111) and Nb(110) samples are presented. © *2006 American Institute of Physics.* [DOI: 10.1063/1.2213171]

I. INTRODUCTION

Since the introduction of scanning tunneling microscope (STM) almost 25 years ago, impressive progress has been achieved with respect to the performance of the microscopes by improving their design with special focus on scanning and approach mechanisms as well as on vibrational decoupling.[1] Those aspects, of course, are interrelated, and to obtain an optimized resolution, the optimization of the mechanical stability of a microscope is a necessary condition. A common way to accomplish a vibrationally quiet environment for the STM is the use of actively damped holders of the STM containing cabinet or even putting it on an independent foundation within an existing building. This latter approach, however, in many cases might not be affordable or even principally not feasible. For instance, in our case, the STM is part of a complex ultrahigh vacuum (UHV) system with many mechanical pumps inevitably nearby and with a laboratory in the third floor of a busy building. It is the aim of the present article to demonstrate that despite these demanding environmental conditions, a hither to unequalled stability of a low-temperature UHV STM could be achieved by design optimization, which translates into an extremely high resolution of 0.2 pm_{rms} in the z direction. Additionally, the instrument is cheap and easy to build.

II. SYSTEM DESIGN

A. Chamber system

Though the complete UHV system is not at the focus of this article, the chamber arrangement is briefly sketched here to give an overview of the possibilities available with the STM described below. The UHV system comprises six separately pumped chambers, a preparation chamber, a transfer chamber, a load lock, a plasma chamber, an analysis chamber, and the STM chamber (see Fig. 1). The chambers are arranged along three perpendicular axes which intersect at the center of the transfer chamber. Thus, by introducing three independent transfer rods along these axes with the possibility to hand over a sample from rod to rod within the transfer chamber, a sample can sequentially be brought into all the chambers. It is worth noting that there are eight parking positions for samples within the transfer chamber allowing storage under UHV conditions.

Within the preparation chamber, samples are mounted on a manipulator (Vacuum Generators) with five mechanical degrees of freedom. Additionally, the samples can be cooled down to approximately 85 K by liquid nitrogen and heated to ~1500 °C by a resistive heater. For sample preparation either by cleaning cycles of externally grown single- or polycrystalline bulk samples or by *in situ* depositing thin films, a 5 keV ion gun connected to a controllable gas inlet system (four gas sources) is available as well as several evaporation sources and a rf/dc sputter equipment.

After its transfer into the analysis chamber, the sample is again mounted onto a manipulator offering five mechanical degrees of freedom. Here, samples can be heated to >2000 °C by an especially designed electron bombardment heater. For analysis, the chamber is equipped with a rear view low energy electron diffraction (LEED) system, a quadrupole mass spectrometer for thermal desorption spectroscopy (TDS), and a hemispherical electron-energy analyzer (Specs HSA 3500) combined with an x-ray source (Mg, Al) and a He lamp allowing x-ray and ultraviolet photoelectron spectroscopies (XPS/UPS).

In the plasma chamber, samples can be exposed to a mild oxygen or hydrogen plasma for cleaning/oxidation/reduction of a sample surface.

B. STM chamber and cryostat

The STM chamber is connected to the transfer chamber by edge-welded bellows, which effectively decouple the STM chamber mechanically from the rest of the UHV system. Additionally, for its vibrational decoupling from the floor, the STM chamber is supported by a pneumatic damping system (Physik Instrumente). Once lifted by this pneumatic system, the resonance frequency of the chamber is

[a]Author to whom correspondence should be addressed; electronic mail: berndt.koslowski@uni-ulm.de

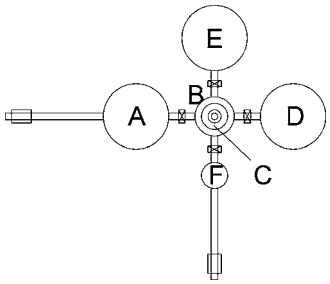

FIG. 1. Schematic of the UHV system: (A) preparation chamber, (B) transfer chamber and parking positions, (C) load lock, (D) analysis chamber, (E) STM chamber, and (F) plasma chamber. The chambers are interconnected by magnetic transfer rods through various valves. As opposed to all others, the STM chamber is vibrationally decoupled by welded bellows and supported by a pneumatic vibration isolation system.

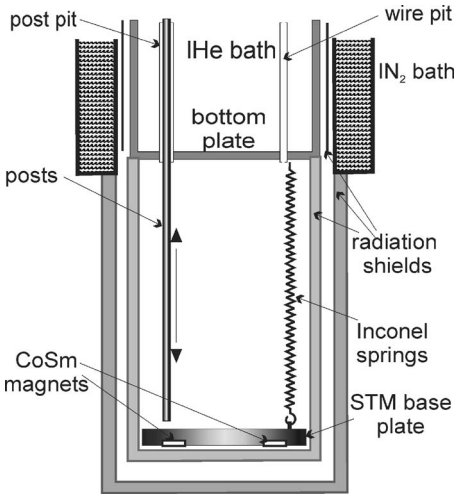

FIG. 2. Schematic of the lower part of the cryostat including the base plate for the STM. Openings with movable shutters within the lower radiation shields allow tip and sample transfer. The upper radiation shield between liquid N_2 and liquid He vessels is cooled by evaporating He from the main reservoir.

<1 Hz. This value is related to the total weight of the STM chamber ($\sim$200 kg), which forms a column of 2.50 m in height comprising an ion getter pump (200 l/s) at the lower end pumping through an additional Ti sublimation pump, the STM chamber supplying electrical connectors, view ports, and a mechanical hand (Vacuum Generators) for sample/tip manipulation, and the cryostat with a liquid N_2 shield (20 l, holding time of $\sim$48 h) and a liquid He reservoir (8 l, holding time of $\sim$36 h). The cryostat is very similar to the one described earlier by Hoffmann *et al.*[2] except for the larger volume of the reservoirs obtained by an increased diameter of the outer tube (30 cm).

For *inside* wiring polyimide-insulated stainless-steel wires (0.1 mm thick) are used, which are led through the liquid He bath (wire pits) to its bottom plate. The wires are anchored at the thermal shields and the bottom plate to guarantee their optimized thermal coupling. At the bottom plate of the liquid He bath, homebuilt electrical connectors facilitate the wiring to the microscope's base plate. Since the wires are susceptible to excess noise signals induced by mechanical distortions via electrofriction along the distance through the liquid He bath to the UHV connectors ($\sim$80 cm), we have installed the most sensitive wire carrying the tunneling current signal I_t along the shortest way out of the UHV system, i.e., through the liquid He and liquid N_2 shields carefully avoiding mechanical contact between the wires' insulation and any other mechanical component. As a consequence, the noise level of the current signal decreased by a factor of at least 10 to below 1 pA as compared to conducting the wire through a wire pit where the wires wiggle uncontrollably (10 pA, temporarily up to 1 nA).

C. STM

The arrangement of various components related to the STM within the cryostat is sketched in Fig. 2. The STM base plate, which is suspended by three Inconel springs, carries the STM itself (described below), a heater ($\sim$1 W), a Cernox resistor for temperature measurement, a tip exchange slot, and the electrical connectors. The resonance frequencies of the seesaw are between 1 and 2 Hz. Two braided wires (Cu, 2.5 mm^2) establish a well defined thermal conductance between the base plate and the bottom plate of the liquid He bath (7 mW/K). This thermal bridge together with the heater allows controlling the temperature of the base plate, which consists of a Cu–mu-metal/Cu–mu-metal/Cu stack and ten magnets (CoSm) of pairwise opposite magnetization arranged on a circle. The magnets damp the seesaw by inducing an eddy current in the liquid He shield. The mu-metal plates hold the magnets and shield the interior with the STM from the corresponding magnetic field. Three posts (linear travel 50 mm) are used to push the base plate of the STM against the bottom of the liquid He shield in order to obtain a faster cooling of the STM or to mechanically fix the seesaw during tip/sample transfer. This way, the STM can be cooled from room temperature to $\sim$10 K within $\sim$4 h. After introducing a new sample at room temperature, it takes about 10–20 min to obtain stable operation of the STM at a temperature <7 K.

Figure 3 sketches the construction of the microscope[3] with the images presented in Fig. 4 illustrating its realization. The main building blocks are three parts made of titanium: the scanner, the sample receptacle, and the body which stiffly connects the scanner and the sample receptacle. Titanium has been chosen because it matches very well the thermal expansion coefficient of macor and the piezos $[(8-9)\times10^{-6}\ K^{-1}]$, it is lightweight making the construction less susceptible to external acceleration, and it is easy to machine. The body also carries the shear-piezo motor (addressed as "1" in Fig. 3) consisting of a quartz-ceramic-steel stack, which allows driving the inertial motion used for the coarse positioning of the scanner/tip. Three stacks are used for a stable three-point bearing of the scanner. An essential component for the inertial motion is the polished sliding area made of molybdenum or a high-speed steel (DIN 1.3344 or 1.3202) without additional coating. Excelling properties of the chosen steel are a high toughness[4] and a low thermal expansion coefficient $[(9-10)\times10^{-6}\ K^{-1}]$ which satisfactorily matches the thermal expansion coefficient of titanium and macor $[(8-9)\times10^{-6}\ K^{-1}]$.[5] Two sliding areas are spark eroded V grooves perpendicular to the sample surface while the third one is

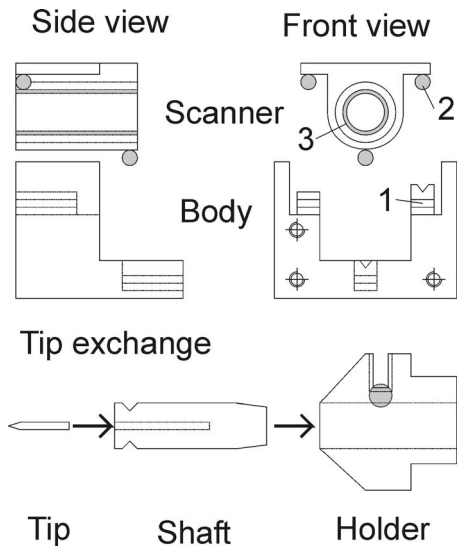

FIG. 3. Schematics of the STM (upper part) and the tip holder (lower part). The sample receptacle (not shown) is screwed to the body with three Mo screws and macor spacers for insulation. Labeled components are (1) shear piezos with insulation and sliding area, (2) sapphire balls, and (3) piezotube.

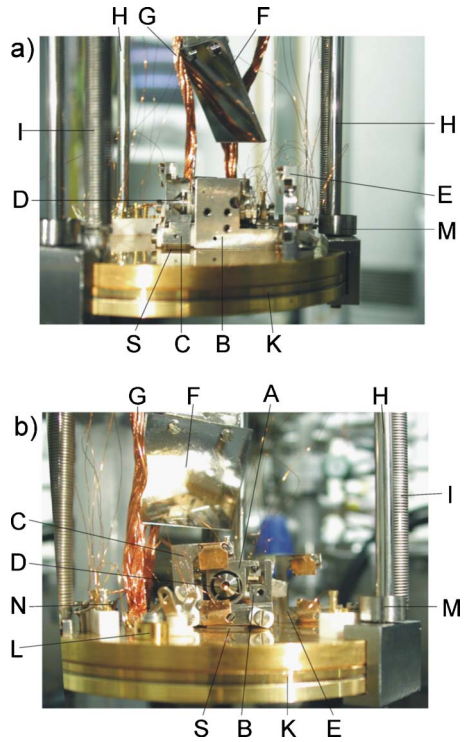

FIG. 4. (Color online) Pictures of the STM on its base plate: (a) side view and (b) front view. The labeled components are (A) scanner including piezotube and tip holder (D), (B) microscope body interconnecting scanner (B) and the sample receptacle (C), (C) sample receptacle with 2 CuBe leaf springs, (D) tip holder, (E) tip-exchange slot, (F) mirror, (G) thermal shunt to the base plate of the He bath, (H) posts moving up/down to free/lock the STM base plate, (I) Inconel springs, (K) microscope base comprising a Cu/mu-metal/Cu/mu-metal/Cu sandwich and the CoSm magnets, (L) Cernox resistor for a four-point temperature measurement, (M) centering screws for the posts, (N) heater (~1 W), and (S) thermal bridge between sample receptacle (C) and base (K).

planar [front left in Fig. 4(a)] since otherwise the scanner position would be overdetermined. The linear travel of the scanner was limited to 7 mm which principally could be extended but appears sufficient in practice.

Three polished sapphire spheres (alternatively tungsten carbide, "2" in Fig. 3)—glued (Polytec H377) to the scanner—constitute the counterpart of the sliding areas. To enhance the contact area between each sphere and its sliding support, the spheres are polished in their final position using diamond paste (grain diameter of 0.25 μm) in order to remove small sectors (some 10 μm in diameter) from the spheres at their contact areas. Without this polish the sliding areas would be ploughed by the spheres and thus destroyed after few experiments. The position of the contact areas have been chosen as to maximize the base area and to minimize the torque exerted to the scanner during inertial motion.

To drive the shear piezos we generate a periodic t^4 signal with t being the time. The driving frequency is around 2 kHz. The two electrodes are supplied by signals of opposite sign to minimize the electrical cross talk to other lines. At room temperature, a driving voltage of ±15 V is sufficient to sustain inertial motion; at low temperatures ±90 V are required. Under these conditions, the velocity of the scanner is ~1 mm/s, and steps of ~40 nm can be generated with satisfactory reproducibility by applying a limited number of cycles.

The piezotube ("3" in Fig. 3) is glued coaxially into the bore of the scanner using a macor spacer at the back end. Similarly, the tip holder (Ti) is glued to the front end of the piezotube again using a macor spacer for insulation. Into the coaxial bore (2.1 mm in diameter) of this holder a cylindrical tip shaft (Mo, diameter of 2.0 mm) is plugged, which holds the actual tunneling tip. The shaft is fixed by another sapphire sphere (diameter of 1.0 mm) and a tungsten spring pushing the shaft against the bottom of the bore. To increase the mechanical stability of the cylindrical shaft within the bore, an ~10 μm deep depression is milled into the wall of the bore opposite to the sapphire ball using a cutting bit of diameter of 1.8 mm. As a consequence, the shaft rests on two rails rather than within the cylindrical fitting. The actual tunneling tip, in most cases made of a tungsten wire (diameter of 0.25 mm), is plugged into a coaxial spark eroded hole (diameter of 0.3 mm) within the shaft. For a safe transfer of the shaft from/to the microscope, there is a circular V groove at the front end matching the tongue of the pincers provided by the mechanical hand. The shaft holding the tip is transferred within the UHV system using an all-molybdenum transfer holder with an integrated complete tip holder, i.e., including sapphire ball and W spring. This arrangement allows heating the tip holder to >2000 °C in the analysis chamber, a necessary prerequisite for a thorough thermal cleaning of the tip.

The receptacle of the sample ("C" in Fig. 4) is mechanically fixed to the STM body by three Mo screws and six macor spacers for insulation. To guarantee a maximum of mechanical stability, the three screws establish a three-point bearing of maximized base area. A further necessary condition is a good thermal contact of the receptacle to the STM base plate, which is achieved by gluing a sapphire plate to the bottom of the receptacle. Counterpart to the receptacle is a transfer holder containing the actual sample. This transfer holder ($13\times13\times2$ mm^3) can be plugged into the receptacle

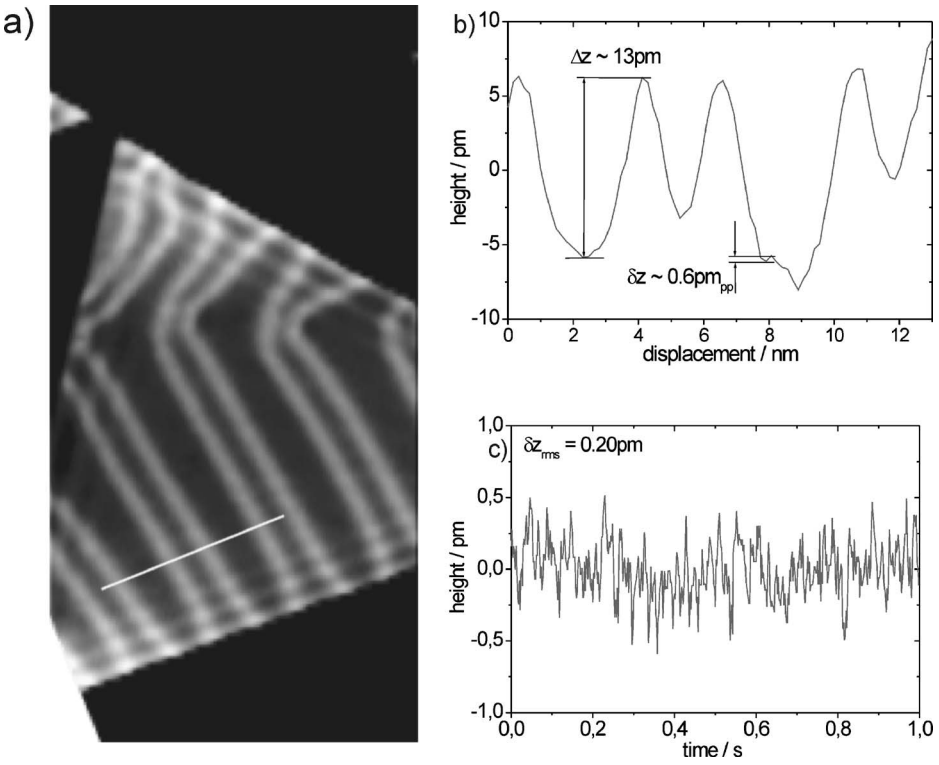

FIG. 5. (a) STM image of a Au(111) terrace on an annealed gold film on glass $(24\times48\times0.020\ \mathrm{nm}^3)$. (b) Cross-section along the line shown in (a) perpendicular to the herringbone structure. The stability of the z signal estimated from the cross section is better than 1 pm. (c) Temporal behavior of the topographic signal z at a fixed (x,y) position within a Au(111) terrace (feedback loop closed). The frequency range of the signal is 0.5–500 Hz and the root mean square δz_{rms} amounts to 0.2 pm. The digitization steps are 40 fm in the present setup.

and it is held there by two CuBe leaf springs (thickness of 0.2 mm). It turned out that these leaf springs are crucial for a stable operation of the STM. They must be strong enough to hold the sample stiffly in place, and they must be weak enough to enable sample transfer. Furthermore, the springs should exert their forces along the vertical symmetry axis of the sample in order to avoid vibrations of the sample if the surfaces of transfer holder and its counterpart are not perfectly parallel. As a result of all the mentioned mechanical precautions, the first resonance frequency of the STM is ~3.5 kHz with lower resonances only present if there is an accidental loose sample mount. To keep this stability, we did not implement a motor drive to move the sample in front of the STM tip. Rather, the sample is positioned manually with the mechanical hand allowing for an effective area of about $1\times4\ \mathrm{mm}^2$ to be analyzed by STM.

III. PERFORMANCE

According to the Cernox resistor the base temperature of the STM is ~6.0 K after cooling with liquid helium. This value, however, represents an upper limit since it is based on a rather rough polynomial interpolation between the two calibration points at 4.2 and 77 K. It is also important to note that the above-mentioned cooling time of about 4 h to reach that temperature starting from 300 K is not sufficient to acceptably suppress thermal drifts. Rather it turns out that approximately one day of keeping the system at nominally 6 K is necessary to achieve a drift ~0.1 pm/s.

To demonstrate the performance of our STM, in Figs. 5 and 6, results of topography as well as spectroscopy measurements are presented taken at 6 K on commercially available thick Au films on glass substrates. Before taking these data, the samples underwent repeated cycles of *in situ* annealing at ~650 °C as well as exposures to a mild hydrogen plasma for surface cleaning.

In Fig. 5(a) one clearly recognizes a Au(111) facet exhibiting the well known $(22\times\sqrt{3})$ herringbone reconstruction.[6,7] The grey scale has been specifically chosen to resolve most clearly this reconstruction, and, consequently, the upper and lower Au terraces are well outside the range of the color table. Additionally, Friedel oscillations are present parallel to the step edges.[8] The corrugation of the herringbone structure along the trace indicated in panel (a) by the solid white line is displayed in panel (b). Quantitatively, one observes a value of 13 $\mathrm{pm}_{\mathrm{pp}}$, which nicely fits to earlier observations.[9] From the noise in Fig. 5(b) one estimates the stability of the topographic signal to be around 0.6 $\mathrm{pm}_{\mathrm{pp}}$. To test the temporal stability of the z signal, a corresponding

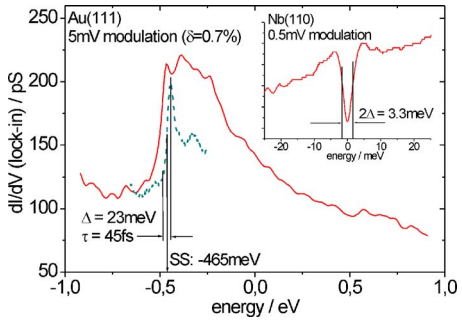

FIG. 6. The differential conductance $\partial I/\partial V$ measured within a small Au(111) terrace. Shown is the average over 40 I-V scans resulting in an error of 0.7%. All the small signatures seen in the differential conductance were reproduced individually by each I-V scan, especially the double peak at the surface state onset which is due to the herringbone reconstruction. The dashed curve showing an even steeper band onset was measured in another terrace. Inset: $\partial I/\partial V$ curve measured on a Nb(110) film at the lowest temperature of the STM exhibiting the signature of the Nb superconducting gap.

time trace is taken on another Au(111) terrace under similar conditions. The result is shown in Fig. 5(c) revealing a peak-to-peak value of 1.0 pm_{pp} corresponding to a root-mean-square noise of 0.20 pm_{rms} on a time scale of 1 s. To the best of our knowledge, this value is unprecedented so far.[10,11]

Figure 6 displays *I-V* spectroscopy data measured on Au(111) terraces as before. Here, 40 *I-V* curves were determined consecutively at a given position to obtain an estimate of the accuracy of the measurement. For the displayed $\partial I/\partial V$-*V* curves an accuracy of 0.7% was found in this way. Consequently, even the small structures in the local density of states (LDOS) below the onset of the surface state at −0.50 and −0.47 eV, respectively, are reproduced accurately in each single *I-V* measurement. In case of the solid LDOS curve, the Shockley-like surface state is resolved including a double peaked structure which is due to the herringbone reconstruction.[12] The detailed fine structure of the surface state varies from terrace to terrace probably reflecting different sizes/shapes/defects. For example, the double peak of the dashed LDOS curve in Fig. 6 taken on a different terrace clearly disappeared while the step indicating the onset of the surface band is significantly sharper with a width of 23 meV corresponding to an average electron lifetime of 43 fs. These values are in excellent agreement with previous measurements.[13,14] To obtain an even better estimate of the energy resolution of our instrument, additionally the superconducting gap of an epitaxially grown Nb(110) film on sapphire[15,16] was determined at 6 K. The corresponding result is presented in the inset of Fig. 6. Clearly, the gap structure on an energy scale of some meV can easily be resolved pointing to a minimum energy resolution of the STM in that range. The visibility of the superconducting gap of the Nb sample furthermore proves that the tunneling tip itself must have adopted a low temperature similar to that of the sample.

In summary, the test measurements presented in the last section demonstrate an extreme high stability of the introduced STM. We believe that this result could be accomplished only by rigorously adhering to basic design principles such as to make it small, lightweight, and rigid and avoid overdetermination.

ACKNOWLEDGMENTS

The authors gratefully acknowledge generous support by the Deutsche Forschungsgemeinschaft (DFG, cooperative research center SFB 569). The authors also thank R. Berndt and J. Kröger for support concerning the construction of the cryostat and K. Wandelt and S. Degen for helpful discussions.

[1] R. Wiesendanger, *Scanning Probe Microscopy and Spectroscopy* (Cambridge University Press, Cambridge, 1994).
[2] G. Hoffmann, J. Kröger, and R. Berndt, Rev. Sci. Instrum. **73**, 305 (2002).
[3] A very early forerunner model has been described briefly in B. Koslowski, S. Strobel, M. J. Wenig, and P. Ziemann, Appl. Phys. A: Mater. Sci. Process. **66**, 1159 (1998).
[4] Toughness is used as the antonym of brittleness and refers to the resistivity against crack formation/propagation. Compare "beam impact test."
[5] According to first experiments, the steel is superior to the molybdenum because the steel is tough and homogeneous. Instead, the molybdenum is brittle and less homogeneous. The lower hardness of the steel reduces the load of the contact areas and the toughness avoids crack formation. Yet, however, there is no sufficient long-term experience on the wear of the steel components.
[6] D. Fujita, K. Amemiya, T. Yakabe, H. Nejoh, T. Sato, and M. Iwatsuki, Phys. Rev. Lett. **78**, 3904 (1997).
[7] D. Fujita, K. Amemiya, T. Yakabe, H. Nejoh, T. Sato, and M. Iwatsuki, Surf. Sci. **423**, 160 (1999).
[8] Y. Hasegawa and Ph. Avouris, Phys. Rev. Lett. **71**, 1071 (1993).
[9] J. V. Barth, H. Brune, G. Ertl, and R. J. Behm, Phys. Rev. B **42**, 9307 (1990).
[10] S. H. Pan, E. W. Hudson, and J. C. Davis, Rev. Sci. Instrum. **70**, 1459 (1999).
[11] J. H. Ferris, J. G. Kushmerick, J. A. Johnson, M. G. Yoshikawa, R. B. Kessinger, H. F. Kingsbury, and P. S. Weiss, Rev. Sci. Instrum. **69**, 2691 (1998).
[12] W. Chen, V. Madhavan, T. Jamneala, and M. F. Crommie, Phys. Rev. Lett. **80**, 1469 (1999).
[13] J. Li, W.-D. Schneider, R. Berndt, O. Bryant, and S. Crampin, Phys. Rev. Lett. **81**, 4464 (1998).
[14] J. Kliewer, R. Berndt, E. V. Chulkov, V. M. Silkin, P. M. Echenique, and S. Crampin, Science **288**, 1399 (2000).
[15] C. Dietrich, H.-G. Boyen, and B. Koslowski, J. Appl. Phys. **94**, 1478 (2003).
[16] B. Koslowski, C. Dietrich, and P. Ziemann, Surf. Sci. **557**, 255 (2004).